MedCrave
Step into the World of Research
Journal of Analytical & Pharmaceutical research

Research Article
Open Access
CrossMark

Synthesis; spectral, computational studies; and antimicrobial evaluations of Fe(II) and Zn(II) chelates containing R'C-NR" and N_2O_2 moieties

Abstract

Mixed M^{2+} chelates; [M(L)(B)(X)] (M=Fe plus Zn; L=Schiff base chelator; B=2'-bipyridine; and X=SO_4/OAc) were synthesized through reflux processes from naphthoquinone chelator, 2-(4,6-dimethylpyrimidin-2-ylamino)naphthalene-1,4-dione, 2,2'-bipyridine plus divalent Fe-sulphate and Zn-acetate salts. The chelator with its chelates were characterized using micro (C,H,N,S) analysis, melting point, magnetic susceptibility plus conductivity assessments; vibrational (FT-IR), electronic (UV-vis), nuclear magnetic resonance (^{1}H and ^{13}C-NMR) and mass (ESI-MS) spectral measurements. The spectral evaluations gave credence to the structural assemblage of the chelator, as well as validates its bi-dentate chelation to the metallic ions through keto-imine (secondary amine) nitrogen and the aromatic ketonic oxygen atoms. Acquired C,H,N,S, Uv-vis, FT-IR and magnetic moment data gave proof of octahedral geometry for the metal chelates, while their neutrality was confirmed by the very low molar conductance values (9.38-12.0 $\Omega^{-1}mol^{-1}$ cm^2) obtained. The stereochemistry of the chelates was further examined through DFT calculations as well as their thermodynamic plus electronic parameters. Acquired antimicrobial values for the synthesized compounds against *P. aeruginosa, S. aureus, B. cereus, E. coli, K. oxytoca*, *P. mirabisis, A. flevus, A. niger* plus *R, Stolonifer* microbes presented convincing evidences to the fact that the chelates remained better anti-bacterial/anti-fungal agents than their chelator. Similarly, the capability of the chelator got enhanced noticeably after chelation with the metallic species, proving the chelates as efficient 1-diphenyl-2-picrylhydrazyl (DPPH) radical scavengers. The molecular docking evaluation verified the compounds as inhibitors of the adopted protein drug targets.

Keywords: chelation, naphthoquinone, 2,2'-bipyridine, antimicrobial, DFT and molecular docking

Volume 11 Issue 2 - 2022

Festus Chioma,[1] Ima Bright Nwoke and,[1] Osi Valentine[1,2]
[1]Department of Chemistry, Ignatius Ajuru University of Education, Rumuolumeni, Rivers State, Nigeria
[2]Physical Chemistry Unit, Department of Chemistry, University of Ibadan, Oyo State, Nigeria

Correspondence: Festus Chioma, Department of Chemistry, Ignatius Ajuru University of Education, Rumuolumeni, Rivers State, Nigeria,
Email chidebestokwu80@gmail.com, festchi@yahoo.com

Received: February 26, 2021 | **Published:** March 30, 2022

Introduction

In recent times, microbial infections have been on a surge against countless known antibiotics hence coaxing health-care consultants to pursue improved pharmacological alternatives.[1–3] Even so, the usage of non-synthetic medicines as antibiotic agents for cure of microbial aliments has been incorporated as an efficient pharmacological possibility. Schiff bases (SBs) remains as such compounds consisting of fundamental molecular frameworks often detected in non-synthetic antibiotics.[4–5] SBs consisting of amino-pyrimidine moiety have an established range of biological actions arising from the existence of the –N=CH– functional group as well as their capability to chelate to metallic species[6–9] forming chelate compounds with improved biological potentials.[10] Chelate metallic compounds of amino-pyrimidine SBs have remained expansively researched on, owing to their value-added pharmacological features when likened to precursor chelator-SBs. The latter is associated with chelation effect known for enhancing lipophilicity in chelate compounds.[11] Improved biotic potentials of the latter remains attributable to the presence of heteroatoms in addition to metallic atoms chelated to biologically lively compounds.[12] Besides enhanced biological actions of chelate-metallic compounds over their forerunner chelators, chelation correspondingly leads to establishment of a better and stable metallic-organic structure. Metal-carbon-based chelation macromolecules displays extraordinary stability when likened to their distinct metal-chelates owing to their chelate influence.

Amino-pyrimidine SBs, as bi-dentate chelators with triple *N*-atoms within their structural units have effusively been adopted in coordination chemistry due to their strong reduction-oxidation equilibrium as well as comparative easiness of functionalization.[13] Metallic chelates incorporating amino-pyrimidine SBs have been described as effective genotoxicity, antineoplastic, antitumor, cytotoxicity, and bactericidal agents.[14] Prior to this, our research group had reported a variety of microbiologically active pyrimidine-based SB metallic chelates.[9,15,16] The enhanced biological potentials of metallic chelates compared to their precursor chelators propelled this current research on metallic chelates of a SB bearing amino-pyrimidine as part of its structural moiety. The electronic, stereo-chemical, plus magnetic-susceptibility of the amino-pyrimidine SB compounds stood examined adopting different analytical, spectral plus theoretical techniques. The in-vitro antimicrobial in addition to antioxidant actions of all synthesized compounds were apprised. Additionally, molecular docking studies (MDS) was employed to appraise the molecular interactions of the chelates with designated drug targets adopting "urate oxidase" of *Aspergillus favus* sort in addition to humanoid haematopoietic cell kinase-Hck in place of drug targets to assess the anti-fungal as well as antioxidant actions of all synthesized chelates independently.[17]

Materials and methods

Materials

Completely, all reagents; 2-hydroxyl-1,4-naphthoquinone (H-NQ), 2,2'-bipyridine (bipy), 2-amno-4,6-dimethypyrimidine (A-DMP), Fe^{2+}-sulphate.$7H_2O$ and Cu^{2+}acetate.H_2O were acquired from stores of Sigma-Aldrich and used with no further purifications. All solvents;

C_2H_5OH, CH_3OH, CH_3COOH, $(CH_3)_3N$, $(CH_3)_2SO$, CH_2Cl_2, were bought from BDH Ltd and used as acquired.

Physical measurements

The Electrospray Ionization Mass Spectrometry (ESI-MS) of the Schiff base was acquired following the procedure earlier documented by our research group.[2,18] Non-modified melting points for the metallic chelates as well as the SB chelator stood acquired via a see-through cut-glass capillary hose on Electro-thermal Temp-Mel melting point machine. The basic contents of carbon, hydrogen, nitrogen were obtained on a Perkin Elmer Thermofinigan flash-(CHN-2400). The vibrational spectra within 4000-350 cm^{-1} range remained obtained as K-Br pellets using Perkin–Elmer Fourier-Transform Infrared Spectrum BX spectrophotometer. The proton (^1H) and carbon-13 (^{13}C) nuclear magnetic resonance (NMR) spectra were acquired at room temperature in *d6*-DMSO with reference to tetramethylsilane (TMS) on 600 MHz Bruker Avance III NMR spectrophotometer. The ultra-violet (UV, 190-400 nm) and Visible (vis, 400-900 nm) spectra were gotten using Perkin-Elmer k20 UV–Vis spectrophotometer. The magnetic susceptibility and molar conductance values were acquired following the procedure reported by Festus et al.[2]

Synthesis

Synthesis of HL chelator

A mixture of 2000 mg (11.484 mmols) of H-NQ, 1414 mg (11.484 mmols) of A-DMP in 20 mL CH_3OH solution and 6 droplets of CH_3COOH was refluxed (6 hr) at ± 54-57°C. The subsequent brown-shade products on refrigerating to 10 °C were filtered, re-crystallized from warm CH_3OH, dried and kept in desiccator. Yield = 2390 mg, f.m(g/mol): 279.296; 68.15 %. mp: 214-216 °C; CHN $C_{16}H_{13}N_3O_2$ (%)-Exp.(Theo): C, 69.05 (69.83), H, 4.78 (4.71), N, 15.13, (15.07); IR(KBr) ν/cm^{-1}: Nitrogen-Hydrogen (3539b), Carbon=Oxygen (1678s), Carbon=Nitrogen (1641s), Carbon=Carbon (1652s), Carbon-Nitrogen (1579s), Carbon-Carbon (1459s), Carbon-Oxygen (1384s), δCarbon-Hydrogen (982s); electronic (cm^{-1}): $\pi\rightarrow\pi^*$ (33580, 30055), $n\rightarrow\pi^*$ (26350, 21280); ^1H-: δ ppm (MHz) 300, *d6*-DMSO): s, 6H, CH_3 (3.3), *d*, 1H, H_5 (6.7); *d*, 1H, H_{17} (7.8); *d*, 1H, H_{12} (7.1-7.3);. *d*, 1H, H_{16} (7.5); *d*, 1H, H_{15} (7.6); *s*, 1H, H_9 (8.1); *s*, 1H, H_{10} (7.3); *s*, 1H, O-H (14.4); s, 1H, HC=N (9.6); ^{13}C-NMR : δ ppm (MHz) 300, *d6*-DMSO): C_9 (108.1); C_{10} (141.3); $C_{18,11}$ (129.2-129.5); $C_{17,12}$ (116.9); $C_{16,13}$ (126.3); and $C_{15,14}$ (124.5); C_8 (153.4); C_2 (182.9); $C_{4,6}$ (168.7); C_5 (119.3) and $C_{19,20}$ (23.4).

Synthesis of the metallic chelates

The synthetic processes of all metallic chelates adopted a literature route.[9] Initially, an CH_3CH_2OH solution (15 mL) of the chelator; HL was gradually added to a stirred CH_3CH_2OH solution (15 mL) of Fe(II) sulphate and; Zn(II) acetate salts separately. These was promptly followed by drop-wise addition of equal-mole of bipy to afford a molar ratio of 1:1:1. The resulting mix was buffered using $(C_2H_5)_3N$, refluxed for 4 hr and cooled to 27°C. Precipitated solid products were acquired on filtration, washed with CH_3CH_2OH and dehydrated in the desiccator under $CaCl_2$.

[Fe(L)(B)(SO_4)]. Colour: brown; f.m(g/mol): 586.352; yield: 52.10%; m.p: 298-301 °C. IR(KBr) ν/cm^{-1}: 3430b ν(O–H), 1674s (C=O), 1629s ν(C=N), 1591s ν(C=C), 1563s ν(C-N), 1475s ν(C-C), 1273s ν(C-O), 1015s δ(C-H), 501s ν(M–N), 457s ν(M–O).CHNSFe ([$FeC_{26}H_{20}N_5O_6S$], %)-Exp.(Theo): C, 53.32 (53.28); H, 3.52 (3.48); N, 12.04 (11.97); S, 5.49 (5.48). Fe, 9.75 (9.59); electronic (cm^{-1}): 26880, 24030 ($n\rightarrow\pi^*$), 36830, 31205 ($\pi\rightarrow\pi^*$), 22760 ($^5T_{2g}\rightarrow{}^5A_{1g}$), 19160 ($^5T_{2g}\rightarrow{}^5B_{1g}$), 12594 ($^5T_{2g}\rightarrow{}^5B_{2g}$). $\Omega^{-1}mol^{-1}$ cm^2: 9.38. μeff (BM): 5.71.

[Zn(L)(B)(OAc)]. Colour: red; f.m(g/mol): 558.884; yield: 74.30%; m.p: 295-297°C. IR(KBr) ν/ cm^{-1}: 1683 (C=O), 1632s ν(C=N), 1584s ν(C=C), 1561s ν(C-N), 1442s ν(C-C), 1270s ν(C-O), 992s δ(C-H), 504s ν(M–N), 421s ν(M–O). CHNZn ([Zn $C_{28}H_{23}N_5O_4$], %)-Exp. (Theo): C, 66.03 (65.88); H, 4.29 (4.19); N, 12.60 (12.57); Cu, 11.81 (11.77). electronic (cm^{-1}): 26880 ($n\rightarrow\pi^*$), 35045 ($\pi\rightarrow\pi^*$), 20040 (M→L). $\Omega^{-1}mol^{-1}$ cm^2: 12.9. μeff (BM): 0.21.

Antimicrobial studies

The keto-imine tautomer chelator, HL and its Fe^{2+} and Zn^{2+} chelates were appraised for antibacterial as well as anti-fungal possibilities against *P. aeruginosa, S. aureus, B. cereus, E. coli, K. oxytoca*, *P. mirabisis, A. flevus, A. niger* plus *R, Stolonifer* species. Assessment methodologies followed that in literature.[11] The well-agar diffusion along with disc procedures remained clearly used for the distinct evaluations. Nutrient agar medium was accepted for the culture of the bacteriological species (37°C; 24 h) maintaining a density of 0.5 McFarland usual units. Equally, potato dextrose agar (PDA) stood as the anti-fungal appraisal media. Using sterilized cotton swabs, all test cultures were evenly inoculated on the Mueller–Hinton agar/ PDA discs surfaces. Into a 6 mm wells bored on the solidified agar/ PDA, 10^6 CFU/mL DMSO solution of separate test compound was poured. At 35°C, incubation was obtained for 24/48 h at 30 min of equilibration. The zones of inhibition growth were acquired from dual replicates of a separate compound. The DMSO solvent functioned as a non-positive control, whereas the drugs; ciprofloxacin as well as fluconazole were adopted as non-negative controls.

Antioxidant studies

The anti-oxidant potentials of the chelator, HL was appraised via ferrous ion chelating ability (FICA) following a literature method.[15] The dilutions; 50, 100 and 200 µg/mL of HL prepared using CH_3OH with ±1 mL of separate solution were gradually introduced into a 100 mL flask. Separately, pre-dissolved 1 mL of 300 µg of $FeSO_4\cdot7H_2O$ and 1 mL of 500 µg of ferrocene were poured into the flask. DMSO was adopted to make up the resultant mixture to 4 mL; and incubated for 15 min at 29°C with absorbance taken at 546 nm. Roughly 3 mL CH_3OH was employed as blank, while the mixture above served as control. Ascorbic acid served as the standard drug. The FICA for the chelator as obtained using % scavenging inhibition = *(Ac–As)/Ac × 100.* Additionally, DPPH appraisal technique was chosen to study the anti-oxidant ability of the chelator alongside its metallic chelators following our preceding reported study[19]. About 0.4 mL of the individual samples in DMSO (50, 100 or 200 µg/mL) was introduced into a 2.6 mL of 0.025 g/L of DMSO pre-dissolved in DMSO. The mixture was intensely shaken, kept for equilibration at 29°C in the dim for 30 mins. Absorbance was taken at 517 against the blank. Practically, 3 mL of DPPH in DMSO plus ascorbic acid were adopted as control as well as standard separately. Trio-testing were taken for every test sample.

Computational studies

The computational studies applied in this study were molecular docking studies and the quantum chemical calculations.

Molecular docking studies

The molecular docking studies is a technique for the investigation of inhibition potentials in compounds. The protein structures of *P. aeruginosa* (PDB ID: 6p8u)*, S. aureus* (PDB ID:2dhn)*, B. cereus* (PDB ID:1ah7)*, E. coli* (PDB ID:1wxh)*, K. oxytoca* (PDB ID:4a56), *P. mirabisis* (PDB ID:6pzl)*, A. flevus* (PDB ID:2pes)*, A. niger* plus (PDB ID:1ks5) were acquired from the RSCB website but prepared

using Biovia discovery studio. The SB was optimized with guassian 09 but the docking evaluations was via pyrx. The visualization of all acquired data were achieved through pymol in addition to discovery studies.

Quantum chemical studies

This was acquired through the Density functional theory (DFT) calculations. The calculations were carried out using B3LYP/6-31 þ G (d,p) basis for chelator atoms while LANL2DZ stood adopted for metallic species[19] via gaussian 09 software.

Results and discussion

Synthesis

The condensation of 2-hydroxy-1,4-napthoqunone with 2-amino-4,6-dimethylpyrimidine gave the cyclic chelator denoted as HL (Figure 1). The HL chelator experienced an acid catalysis in accordance with documented reports.[9] Keto-imine tautomeric structure was assumed by our synthesized chelator displaying exceptional solubility in organic solvents. The chelator further reacted with sulphate and acetate salts of Fe(II) plus Zn(II) ions to give the metallic chelates (Figure 2). Shades of brown and red were detected for the chelates. The chelator presented strong melting points different from that of the precursor. Equally, the melting points of the metal chelates widely varied from that of the chelator.

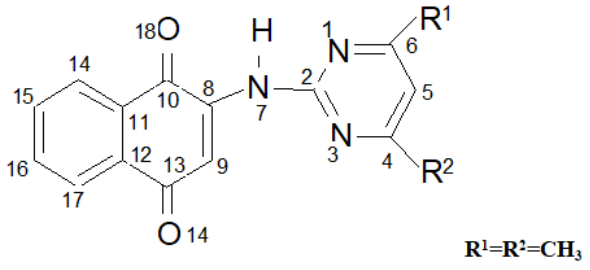

Figure 1 Proposed Structure for Chelator.

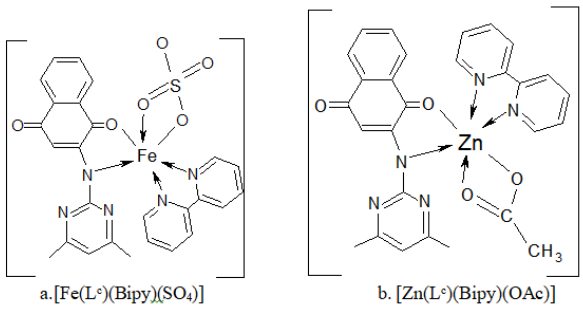

Figure 2 Proposed Structures for the Metal Chelates.

Elemental plus metal species' ratio contents; and molar conductance estimation

The elemental estimation of carbon, hydrogen, nitrogen and sulphur estimation gave a 1:1 and 1:1:1 proportions for the chelator and its Fe(II) plus Zn(II) chelates. The acquired investigational data deeply conformed to all obtained theoretical values, substantiating the suggested structural assemblages for the synthesized compounds. Principally, the M(II) chelates exhibited room temperature firmness in addition to solvent-less status at distinct settings. Completely, acquired data for metal ions' contents indicates that there exist conformity among the investigational and hypothetical data in percentage metal contents in all chelates. Equally, acquired molar conductance data in the range, 9.38–12.9 ohm^{-1}cm^{2}mol^{-1} depicts 1:1 molar-ionic chelates, as figures greater than 40 ohm^{-1}cm^{2}mol^{-1} plus 90 ohm^{-1}cm^{2}mol^{-1} stand repeatedly linked to 1:1 as well as 2:1 ionic chelates separately.[2,20]

NMR studies

The HL chelator was evaluated with NMR which remained adopted predominantly to ascertain if the chelator was a *keto-* or *enol-* amino-naphthoquinone tautomer in DMSO. All obvious signals within the chelator's spectrum were compared to systems similar moieties reported online.[21,22] The naphthalene hydrogen atoms within HL chelator remained observed around 7.76-7.98 ppm as multiplets, 7.35 ppm as singlet whereas the pyrimidine hydrogen atoms remained singly detected at 6.28 ppm. The NH protons appeared as a broad-like singlet signal at 3.38 ppm whereas the CH_3 protons were noticed as a sharp singlet at 2.49 ppm. The ^{13}CNMR spectrum of HL chelator presented resonance peaks typical of napthoquinone C-atoms (C_{10}, C_{11}, C_{12}, C_{13}, C_{14}, C_{15}, C_{16},$_{17}$, C_{18} plus C_{19}) at 159.6, 111.0, 181.3, 184.7, 131.9, 130.6, 125.4-125.9, 133.2 ppm in addition to 134.5 ppm. The peak at 31.8 was distinctive of the carbon atoms ($C_{7,8}$). Additionally, observed resonance peaks at 156.9 ppm, 106.7 ppm plus 159.6 ppm remained ascribed to C_2, C_5 plus $C_{4'6}$ atoms individually of the pyrimidine ring.

FT-IR data

The appropriate FT-IR spectral bands of Fe(II) as well as Zn(II) chelates together with their chelator were acquired between 350-4000 cm^{-1} and thoughtfully apportioned on association with documented assessments of seminar assemblages.[23] Bands conforming to amino groups repeatedly detected in amino-pyrimidines remained absent in the spectrum of the chelator supporting condensation via amino moiety with the cyclic ketone atoms[21]. The FT-IR spectrum of HL chelator presented sturdy bands at 3536 cm^{-1} which stood assigned to N-H stretching vibration arising from an amide moiety. The band remained broadened due to intra-molecular H-bonding within the chelator. [24] Strong-average H-bands of the cyclic systems, ν(Ar–H), resonated amid 3013 cm^{-1} plus 3001 cm^{-1} in the spectra of the chelates. Likewise, the CH_3 substituent of the HL chelator plus its chelates exhibited regular asymmetric/symmetric stretching vibrations for the alkyl moieties. The *ν*(C=N) noticed as a singular band in the spectrum of the chelator remained as such in the spectra of the metallic chelates specifying Fermi resonance.[25] The chelator further underwent keto-enol tautomeric grouping in solution to offer C=N moiety during complexation.[26] Similarly, the free ν(C=O) stretching vibrations identified as sharp bands at 1678 cm^{-1} moved to lesser/greater wavenumbers in the spectra of the metallic chelates confirming the participation of ketonic *O* atom in complexation. Sharp absorption signals at 1641 cm^{-1}, 1459 cm^{-1} plus 982 cm^{-1} remained apportioned to *ν*(Carbon-Nitrogen) of the cyclic rings, *ν*(C-C) plus *δ*(C-H) signals. In addition, validation of the enol *O* plus imine *N* atoms in chelation to metallic ions were validated by the presence of novel bands owing to ν(M-O) as well as ν(M-N) within the spectra of the chelates.[21] The imine ν(Carbon=Nitrogen) band of the chelator wasn't detected rather Carbon=Nitrogen plus Carbon-Nitrogen vibrational wavelengths of the pyrimidinyl moiety appeared at 1641 and 1579 cm^{-1}. These bands moved to lesser/higher wavelengths within the metallic complexes owing to chelation effect. Correspondingly, the band at 1678 cm^{-1} in the chelator's spectrum, collaborative of ν(C=O) experienced lesser/higher frequency shifts in the metallic byproducts, substantiating the involvement of the carbonyl *O* in complexation to the metallic ions. The newfangled signals noticed within the ranges 504−501 as well as 457−421 cm^{-1} remained allocated to ν(M-N) plus ν(M-O) signals singly.

UV-Vis and magnetic susceptibility studies

The assigning of geometry to our synthesized metal chelates were on the basis of UV-Vis absorption band points in addition to the number of *d-d* transition bands by reference to literature on comparable assemblages.[27–29] Basically, the chelator had absorption at 26350 cm^{-1} and 21280 cm^{-1} with obvious shifts in the chelates which were assigned to n→$\pi*$ transition with C=N moieties. Also, the transition $\pi \rightarrow \pi*$ of the chelator was detected at 33580 cm^{-1} and 30055 cm^{-1} which essentially remained unaffected in the spectra of the metal chelates. These two bands were observed at altered wavenumbers but moved to lower/higher energies upon coordination, signifying chelation of the chelator with the metallic ions.

The ultraviolet spectra of the synthesized iron(II) chelate stood characterized with two bands accredited to $\pi^* \leftarrow n/\pi^* \leftarrow \pi$ and CT transitions, Four coordinate tetrahedral iron chelates are often linked with a lone high spin transition, $^5E \rightarrow {}^5T_2$ ordinarily intense as well as broad owing to electronic wave function plus Jahn Teller effect, while square planar iron complexes are rare. d^6 systems usually exhibit crossover phenomena involving $^5T_{2g}(t_2^4e^2)$ and $^1A_{1g}(t_2^6)$ states principally with Fe(II) chelates comprising N-donor atom chelators.[30] The visible spectrum of [Fe(L)(Bipy)(SO_4)] chelate showed three characteristic bands consistent of $^5T_{2g} \rightarrow {}^5A_{1g}$, $^5T_{2g} \rightarrow {}^5B_{1g}$ and $^5T_{2g} \rightarrow {}^5B_{2g}$ transitions typical of an octahedral geometry.

The electronic spectra of the zinc(II) chelate expectedly presented only charge transfer transitions from M→L at 20040 cm^{-1} for [Zn(L)(Bipy)(OAc)], as no *d-d* transition was expected for d^{10} zinc(II) chelates (Atmaran and Kirian, 2011). Observed bands at the 26880 cm^{-1} and 35045 cm^{-1} region were intra-chelator bands. Divalent zinc possesses $3d^{10}$ electron configuration and exhibits *μeff* values corresponding to zero unpaired electrons. In reported studies, observed *μeff* of 5.0-5.2 B.M are often documented for magnetically dilute iron(II) chelates regardless of stereochemistry with exceptions commonly noticed in spin crossover environs.[30] The synthesized iron(II) chelate presented *μeff* data of 5.71 B.M. which was in agreement with the assigned geometries.[31] Observed *μeff* value of 0.21 B.M. was indicative of diamagnetism for the synthesized zinc(II) chelate and corroborates its assigned stereochemistry geometry.

The ESI-MS studies

The ESI-MS was evaluated for better assessment of the chelator's formula mass as well as to ascertain its mode(s) of fragmentation. The ESI-mass spectrum of HL chelator showed a peak at m/z 301 which might be arising from extra mass unit. The chelator with the condensed formula, $C_{16}H_{13}N_3O_2$ in its mass spectrum presented a molecular ion peak (m^+.) at m/z 278 owing to $(L)^+$. (on loss of H) that agrees to the formula mass of the chelator (Table 1). Outside the latter, the chelator exhibited fragment ion peaks at m/z 251, 237, 175 and 149 consistent with [CO; m/z = 28], [CH_3; m/z = 15], [$C_4H_4N_2$; m/z = 61] and [CHN; m/z = 27] separately.

Table 1 Mass spectra Result for HL Chelator

Ligands	Fragmentation	
	m/e	m/z
HL		278.0 [-H], 251 [-CO, 28]
$C_{16}H_{13}N3O_2$		236 [-CH_3, 15], 175 [-$C_4H_4N_2$, 61]
[279.294]	278.0	148 [-CHN, 27]

Keys: EMU=Extra mass unit

Biological evaluations

The synthesized chelator, HL with its resultant metallic chelators were evaluated against *S. aureus, P. aeruginosa, E. coli, B. cereus, P. mirabilis* plus *K. oxytoca* to ascertain their possibilities as anti-bacterial agents. Adopting growth inhibition zone measurement as standard for evaluation,[19] the anti-bacterial actions of compounds were appraised as accessible in 'Table 2. The chelator as well as chelates largely showed growth inhibitory zones distinctly. The antibacterial result of the chelator and its heteroleptic metallic chelates designate that all synthesized compounds principally displayed actions against all the microbes. As expected, the chelates were substantially more active than the chelators (HL and 2,2'-bipyridine).[29] e.g. all the chelates exhibited good activity than that of the chelators against the microbes; *E. coli* and *P. mirabilis* having inhibitory zones range of 18.0-28.0 mm plus 18.5-28.0 mm. Additionally, Zn(II) and Fe(II) complexes presented broad-spectrum actions larger compared to the chelators as well as ascorbic acid, ciprofloxacin against *P. aeruginosa* (31.0 mm, 31.0 mm, 28.0 mm); *S. aureus* (28.0 mm); and *P. mirabilis* (25.0 mm, plus 28.0 mm) signifying their probable efficiency as broad-spectrum anti-bacteriological agents. The data acquired from the anti-fungal assessment of HL chelator plus its chelates against *A. niger, A. flevus* plus *R. Stolonifer* denotes outstanding to average growth inhibition zones. All fungal organisms were inhibited by HL chelator with enhanced inhibitory growth zones of 11.0–29.0 mm. The actions of the chelator against the assessed organisms remained unpredictably improved compared to the metal chelates.[32] Generally, the chelates had moderate inhibitory zones of 15.5–31.0 mm erratically high susceptible than the metal free chelator Table 3.

Antioxidant studies

The antioxidant capacities of the synthesized chelator was determined by ferrous ion-chelating assay (FICA). The FICA data were generally expressed as equivalent of the standard antioxidant agent (ascorbic acid). The values presented in Table 4 show that the chelator possessed good chelating capacity towards the ferrous ion. The HL had FICA values of 78.76 plus 74.5% and 65.8% separately at concentrations of 200 and 100 mg/mL higher than that of the standard ascorbic acid. The chelator and its chelates were evaluated for free radical scavenging effects with DPPH radical at several concentrations (200, 100 and 50 μg/mL) in 1mL DMSO. Acquired data for the compounds on the basis of percent inhibition as contained in Table 5 denotes that the compounds largely demonstrated actions in DPPH assay. Inhibitory figures typically reveal magnitude of radical scavenging actions. The chelator extensively exhibited percentage inhibitory data lower or comparable to that of ascorbic acid symbolic of their anti-oxidant capacities. The capability of the chelator got enhanced noticeably after coordination with metallic ions. Generally, the chelates presented better DPPH radical scavenging actions. Subsequently, the values of the DPPH anti-oxidant actions verified that the compounds can be adopted for design as well as syntheses of drugs for the treatment of pathological diseases arising from oxidative stress.

Docking results

The docking studies was adopted to appraise the interactions that exists amid the chelator-ligand and the metallic chelates, solely to ascertain how they bounded with the proteins. Table 6 denotes the binding affinities of the compounds with the various microbes. The interaction of the HL chelator and chelates with *S. Aureus* is presented in Figures 3 and 4. Hydrogen bonds' and hydrophobic interactions stood observed to exist amid the proteins and the chelates. The molecular docking studies in no way certifies the effectiveness of a compound over the other but gives an idea of the chelator-protein stability in addition to interactions. Generally, all compounds (HL

and M(II) chelates) possessed little or no electrostatic interactions which signifies a non-suicidal effect. Based on the docking studies, the proposed chelator HL possessed a binding affinity higher than those of the metal chelates with [Fe(L)(Bipy)(SO_4)] being greater than Zn(L)(Bipy)(OAc)]. The bond existing amid the 2,2'-bipyridine and the Zn atom was observed to be non-existent but their existed signs of intermolecular interactions amid them.

Table 2 Antibacterial data of HL Chelator with its M^{2+} chelates

Compound/ Bacteria	Bacillus cereus	Escherichia coli	Klebsilla oxytoca	Pseudomonas aeruginosa	Staphylococcus aureus	Proteus mirabilis
HL	24.5±1.7	16.0±2.8	26.0±2.4	18.0±0.6	11.5.0±0.7	16.0±1.4
[Fe(L)(Bipy)(SO_4)]	15.5±0.7	23.5±0.1	19.0±1.4	31.0±2.1	28.0±1.7	25.0±0.7
[Zn(L)(Bipy)(OAc)]	16.0±0.6	24.5±1.7	21.0±2.1	31.0±0.0	20.0±1.4	28.0±0.0
2,2'-Bipy	15.5 ± 0.7	12.0 ± 2.8	26.0 ± 2.8	8.5 ± 0.7	17.0 ± 4.2	19.5 ± 2.1
+Ciprofloxacin	33.0 ± 3.5	32.0 ± 1.4	36.0 ± 2.8	26.5 ± 0.7	29.0 ± 2.1	23.0 ± 1.4
-DMSO	0.0±0.0	0.0±0.0	0.0±0.0	0.0±0.0	0.0±0.0	0.0±0.0

Table 3 Anti-fungal Result for HL Chelator with its M^{2+} chelates

Fungal/Compounds	Aspergillus niger	Aspergillus flevus	Rhizopus Stolonifer
HL	23±0.3	29±1.4	27±0.7
[Fe(L)(Bipy)(SO_4)]	11±1.4	17±0.7	13±0.0
[Zn(L)(Bipy)(OAc)]	11±1.4	19±2.1	-
2,2'-Bipy	16±1.6	19±1.4	13±0.7
+ Fluconazole	36±0.3	29±0.7	38±0.3
-DMSO	-	-	-

Table 4 Ferrous Chelating Data of the HL Chelator

Compounds	Concentration	Absorbance			Mean (Error)	% Inhibition (Error)
		1	2	3		
Blank	-	0.169	0.17	0.168	-	-
	Ic_{50}	0.029	0.03	0.029	0.056(±0.004)	65.8(±2.43)
HL	Ic_{100}	0.022	0.021	0.022	0.063(±0.003)	74.5(±0.45)
	Ic_{200}	0.017	0.019	0.018	0.067(±0.004)	78.76(±2.12)
Standard	Ic_{50}	0.039	0.038	0.039	0.046(±0.003)	53.96(±1.86)
Ascorbic Acid	Ic_{100}	0.035	0.036	0.037	0.049(±0.004)	57.33(±2.41)
	Ic_{200}	0.027	0.029	0.03	0.056(±0.004)	66.2(±2.72)

Table 5 DPPH radical Scavenging data of HL Chelator with its M^{2+} chelates

Compounds	Concentration	Absorbance			Mean (Error)	% Inhibition (Error)
		1	2	3		
Blank	-	0.669	0.67	0.671	-	-
HL	Ic_{50}	0.281	0.283	0.281	0.388(±0.001)	57.96(±0.15)
	Ic_{100}	0.131	0.131	0.126	0.540(±0.003)	80.66(±0.46)
	Ic_{200}	0.111	0.111	0.113	0.557(±0.000)	83.23(±0.15)
[Fe(L)(Bipy)(SO4)]	Ic_{50}	0.025	0.026	0.027	0.644(±0.000)	96.13(±0.15)
	Ic_{100}	0.01	0.011	0.01	0.659(±0.001)	98.46(±0.07)
	Ic_{200}	0.001	0.002	0.003	0.668(±0.000)	99.73(±0.15)
[Zn(L)(Bipy)(OAc)]	Ic_{50}	0.205	0.206	0.207	0.464(±0.000)	69.30(±0.10)
	Ic_{100}	0.089	0.091	0.092	0.579(±0.000)	86.46(±0.21)
	Ic_{200}	0.074	0.075	0.073	0.596(±0.001)	88.93(±0.15)
2,2'-Bipy	Ic_{50}	0.172	0.17	0.168	0.501(±0.004)	74.76(±0.570)
	Ic_{100}	0.16	0.16	0.158	0.510(±0.002)	76.23(±0.234)
	Ic_{200}	0.152	0.152	0.15	0.518(±0.002)	77.40(±0.173)
	Ic_{50}	0.093	0.089	0.094	0.578(±0.002)	86.26(±0.38)
Standard	Ic_{100}	0.085	0.081	0.082	0.587(±0.002)	87.66(±0.32)
Ascorbic Acid	Ic_{200}	0.078	0.074	0.076	0.594(±0.002)	88.67(±0.35)

Table 6 Binding Affinities in (kcal mol-1) of the HL chelate and its complexes with various microbes obtained from docking studies

Microbes	HL Chelator	[Zn(L)(Bipy)(OAc)]	[Fe(L)(Bipy)(SO_4)]
B. Cereus	-7.7	-10.2	-9.6
A. niger	-7.9	-8.8	-10
E. Coli	-8	-9.3	-9.3
S. Aureus	-6.8	-8.9	-8
A. flevus	-7.7	-9.5	-9.6
K. Oxytoca	-6.9	-8.6	-8.7
P. Aeruginosa	-8.9	-8.2	-8.2
P. Mirabisis	-6.6	-8.2	-8.2

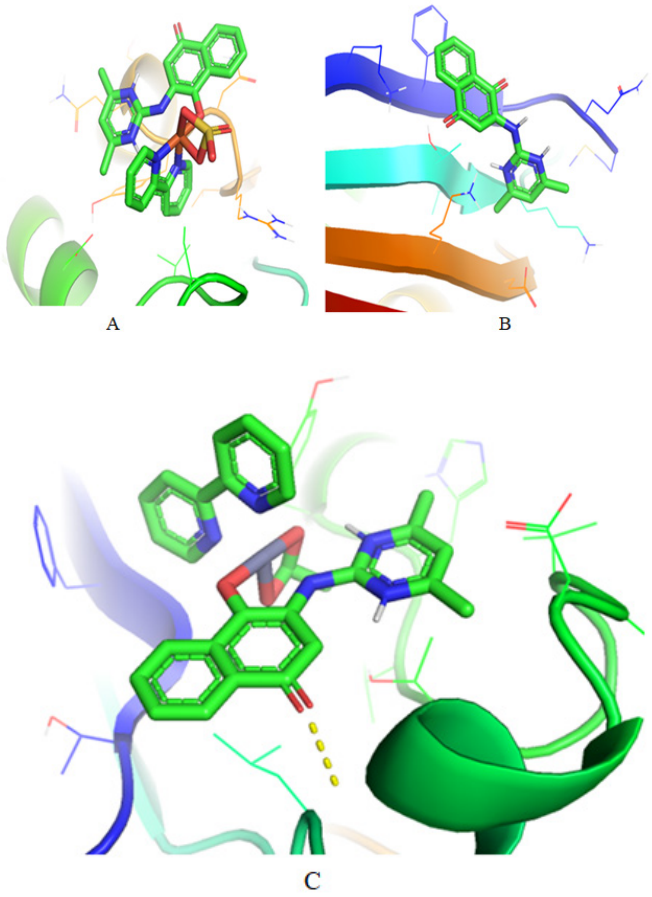

Figure 3 Interaction between the compounds and proteins a) [Fe(L)(Bipy)(SO_4)]; (b) HL Chelate; (c) Zn(L)(Bipy)(OAc)].

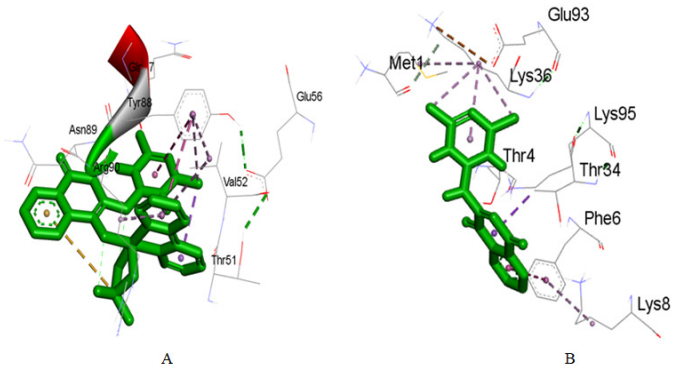

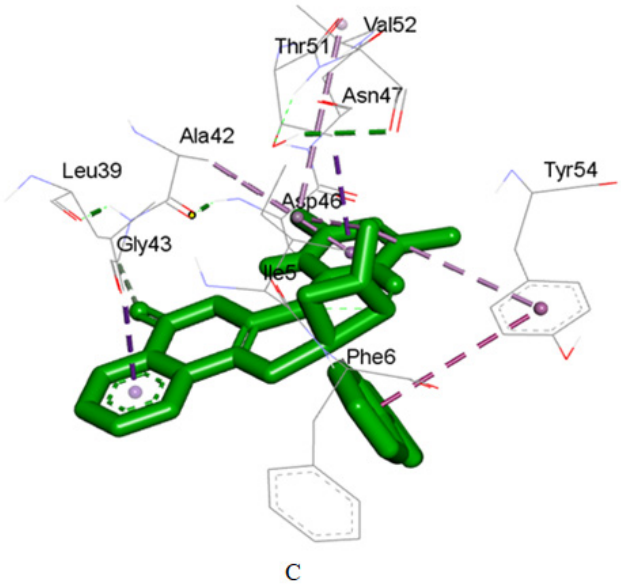

Figure 4 Interaction between the compounds and proteins showing the binding sites and target proteins (a) [Fe(L)(Bipy)(SO_4)]; (b) HL Chelator; (c) [Zn(L)(Bipy)(OAc)].

The frontier molecular orbitals

The optimized structures; and the HOMO plus LUMO diagrams are given in Figure 5–13. The frontier molecular orbitals theory has become very useful in the identification of possible sites for electron transfer amid molecules and its biological targets.[33] The HOMO depicts the electron donating ability of a compound while the LUMO depicts the electron accepting ability of a compound. Higher HOMO values favors electron donation while lower LUMO favors electron acceptance. Therefore, lower energy HOMO and LUMO energies also illustrate the keenness of a molecule to give and receive electrons respectively.[11,19] From the result as shown in Table 7, the HL chelator had lowest HOMO energy and the highest LUMO signifying a higher energy gap which might make the keenness of electron reception difficult. Complexation reduced drastically the energy gap, which suggest easy flow of electrons from the complex and whatever system it is integrating with.

Chemical reactivity describes the tendency of substances to undergo chemical reactions Table 8.[34] The E_{HOMO} and E_{LUMO} values are useful in the determination of several other reactivity parameters like ionization potential, electron affinity, electronegativity, hardness and softness. The relationship of these parameters with the HOMO and LUMO and with one another has been mentioned in various literatures.[33–35] The

electron affinity depicts the amount of energy required for a ligand to accept electrons, the ionization potential represents the capacity of a ligand to donate electrons, and the hardness measures the resistance of an atom to a charge transfer while the softness describes the capacity of a ligand to receive electrons. In general, a hard molecule has the least tendency of reaction while a soft molecule has a greater tendency of reacting. The electrophilicity is now considered a better descriptor of overall chemical reactivity because it provides information on both the hardness and chemical potential of a substance. Higher values of the electrophilicity is an indication of the substance of being a better electrophile while lower electrophilicity values indicates nucleophilic ability. A higher electrophilic values indicates higher chemical reactivity which also places the metal chelates ahead of the HL.[36] This makes [Fe(L)(Bipy)(SO4)] better substance than [Zn(L)(Bipy)(OAc)] and generally making metal chelates better options for drugs than the chelator itself because of the ease of electron transfer associated with the chelates.

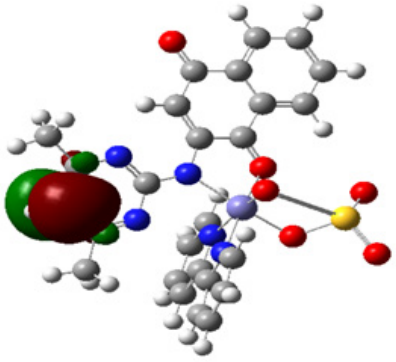

Figure 5 Fe(II) Chelate HOMO Structure.

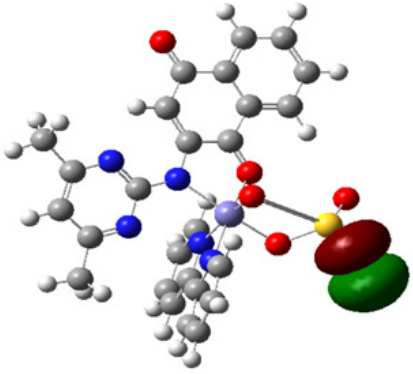

Figure 6 Fe(II) Chelate LUMO Structure.

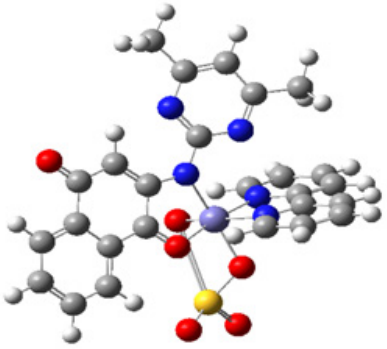

Figure 7 Fe(II) Chelate optimized Structure.

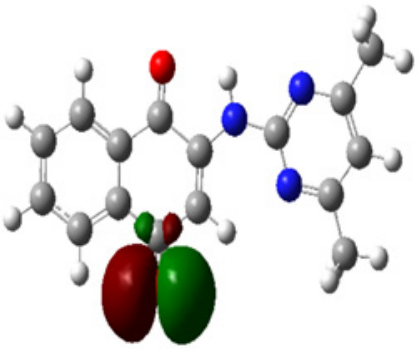

Figure 8 The Chelator HOMO Structure.

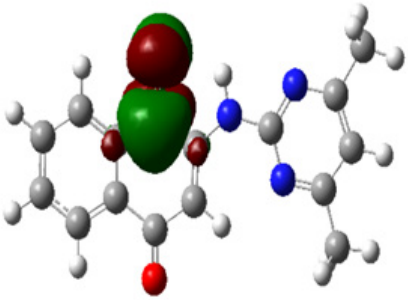

Figure 9 Chelator LUMO Structure.

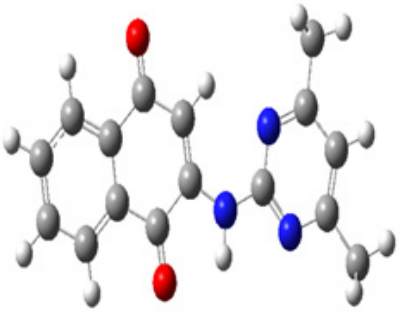

Figure 10 Optimized Chelator Structure.

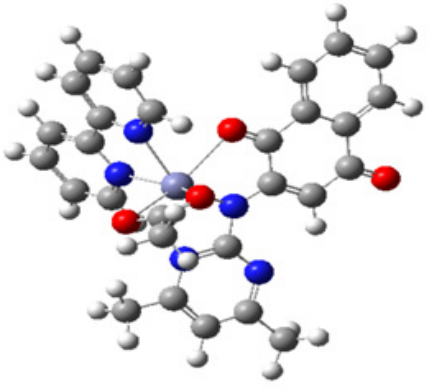

Figure 11 Zn(II) Chelate optimized Structure.

Citation: Chioma F, Nwoke IB, Valentine O. Synthesis; spectral, computational studies; and antimicrobial evaluations of Fe(II) and Zn(II) chelates containing R'C-NR" and N_2O_2 moieties. *J Anal Pharm Res.* 2022;11(2):45–54. DOI: 10.15406/japlr.2022.11.00401

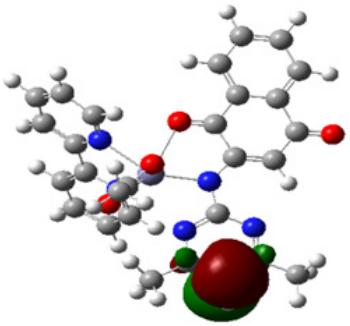

Figure 12 Zn(II) Chelate HOMO Structure.

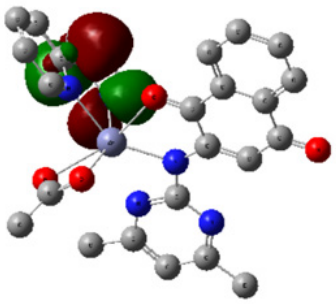

Figure 13 Zn(II) Chelate LUMO Structure.

Table 7 Global Parameters

Parameters	HL Chelator	[Fe(L)(Bipy)(SO4)]	[Zn(L)(Bipy)(OAc)]
Dipole (Debye)	2.3705	12.1098	10.6529
EHOMO (ev)	-7.13726	-4.2846	-3.14726
ELUMO (ev)	-0.38349	-3.1578	-1.2226
ENERGY GAP	6.75377	1.12684	1.92466
Ionization energy	7.13726	4.2846	3.14726
Electron affinity	0.38349	3.1578	1.2226
Electronegativity	3.7683	3.7208	2.1849
Hardness	3.3769	0.5638	8.9623
Softness	0.14806	0.8868	0.51957
Electrophilicity	2.09363	12.277	2.4809

Table 8 Geometry; Bond Length

HL Chelator Bond length (A0)		[Fe(L)(Bipy)(SO4)]		[Zn(L)(Bipy)(OAc)]	
C10-O16	1.2293	C10-O16	1.27879	C10-O16	1.26161
		Fe34-O16	1.94402	Zn34-O16	2.44859
		Fe34-N18	2.0236	Zn 34-N18	2.1121
		Fe34-N53	1.96983	Zn 34-N53	2.23278
		Fe34-N54	2.04891	Zn 34-N54	2.22762
		Fe34-O55	1.66109	Zn 34-O55	2.10724
		Fe34-O56	1.93451	Zn 34-O56	2.44086
Angles					
C13-C10-C4	118.124	C13-C10-C4	122.624	C13-C10-C4	119.32
C13-N18-C20	131.547	C19-N18-C13	123.286	C19-N18-C13	127.363
N21-C20-N22	26.606	N20-C19-N21	28.331	N20-C19-N21	27.813
		N18-Fe34-O16	48.163	N18-Zn34-O16	49.022
		055-Fe34-056	45.837	055-Zn34-056	68.563
		N53-Fe34-N54	48.384	N53-Zn34-N54	53.271
		C35-N54-C39	29.781	C36-N54-C48	29.803
		C44-N53-C45	120.53	C44-N54-C48	120.601
Dihedral Angles					
		Fe34-055-056-S59	19.144	Zn34-O55-O56-C57	3.269

Complexation affected the geometry of the chelates. The type of metal in the centre did not affect the geometry in general as each metal chelate where observed to be showing similar geometries based on values obtained from bond length and bond angles. But an outstanding difference was observed in the dihedral angles of Zn -OOC and Fe-OOS all these are illustrated in Table 7. A possible reason might be due the large difference in electronegativity between S and C. The Bond length has an inverse relationship with bond energies and a direct relationship with chemical reactivity hence the reason why the metal chelates are more reactive as seen from the docking studies.

Conclusion

This current study reports the syntheses of new metal chelates of Fe(II) plus Cu(II) as well as their chelator Schiff base acquired from 2-hydroxyl-1,4-naphthoquinone and 2-amno-4,6-dimethypyrimidine through reflux-condensation process. The synthesized compounds were characterized using analytical, spectral and theoretical methods. Spectral evaluations gave credence to the structural assemblage of the chelator, as well as validates its bi-dentate chelation to the metallic ions through keto-imine (secondary amine) nitrogen and the aromatic ketonic oxygen atom. The metallic chelates adopted

octahedral structure on the basis of vibrational plus electronic data; and magnetic susceptibility values. The stereochemistry of the chelates was examined through DFT calculations in addition to their thermodynamic plus electronic parameters. Acquired antimicrobial values for the synthesized compounds presents convincing evidences to the fact that the chelates remained better antibacterial/anti-fungal agents than their chelator. Similarly, the capability of the chelator got enhanced noticeably after chelation with the metallic species, proving the chelates efficient DPPH radical scavengers. The molecular docking evaluation verified the compounds as inhibitors of the adopted protein drug targets.

Acknowledgements

Authors gladly thank Department for Chemistry, Ignatius Ajuru University of Education for laboratory supports.

Declaration of interests

Wholly, the authors do here state no interest conflict of any sort with regards to the publication of this experimental research article.

Funding

None.

References

1. Sayer JR, Wallden K, Pesnot T, et al. 2- and 3-substituted imidazo [1, 2-a]pyrazines as inhibitors of bacterial type IV secretion. *Bioorg Med Chem.* 2014;22:6459–6470.
2. Festus C, Okafor SN, Ekennia AC. Heteroleptic Metal Complexes of a Pyrimidinyl Based Schiff Base Ligand Incorporating 2,2′-Bipyridine Moiety: Synthesis, Characterization, and Biological Studies. *Front Chem*. 2019;**7**:1–12.
3. Festus C, Okocha O. Behaviour of N-(2-hydroxybenzylidene)pyrazine-2-carboxamide in complexation towards Fe(II), Co(II), Ni(II) and Cu(II) ions: synthesis, spectral characterization, magnetic and antimicrobial properties. *International Journal of Chemistry Pharmacy & Technology*. 2017;2(4):143–153.
4. da Silva CM, da Silva DL, Modolo LV, et al. Schiff bases: a short review of their antimicrobial activities. *J Adv Res.* 2011;2:1–8.
5. Hassan R, Arida H, Montasser M, et al. Synthesis of new Schiff base from natural products for remediation of water pollution with heavy metals in industrial areas. *J Chem.* 2013;2013:1–10.
6. Xiqing ML, Zhang SJ. Synthesis and characterization of a series of novel 2-Schiff base-substituted phenylpyrimidine. *Arab J Chem*. 2017;10:167–171.
7. Ali NN, Khan A, Amir S, et al. Synthesis of Schiff bases derived from 2-hydroxy-1-naphthaldehyde and their Tin(II) complexes for antimicrobial and antioxidant activities. *J Chem Soc Ethiopia*. 2017;31.
8. Sharma S, Jain ADK, Aggarwal A, et al. Synthesis, characterization and pharmacological evaluation of novel Schiff bases of imide moiety. *J Med Sci.* 2012;12:61–69.
9. Festus C. Synthesis, Characterization and Antibacterial Studies of Heteroleptic Co(II), Ni(II), Cu(II) and Zn(II) Complexes of N-(2-hydroxybenzylidene)pyrazine-2-carboxamide. *International Journal of Chemistry, Pharmacy & Technology*. 2017;2:202–211.
10. Lipinski CA. Lead- and drug-like compounds: the rule-of-five revolution. *Drug Discov Today Technol.* 2004;1(4):337–341.
11. Festus C, Jude IA, Collins UI. Ligation Actions of 2-(3-hydroxypyridin-2-ylamino)naphthalen-1,4-dione: Synthesis, Characterization, *In-vitro* Antimicrobial Screening, and Computational Studies. *Indian Journal of Heterocyclic Chemistry*. 2021;31:1–13.
12. Bauer AW, Kirby WMM, Sherries JC, et al. Antibiotic susceptibility testing by a standardized single disk method. *Am J Clin Pathol*. 1999;45:493–4965.
13. Selvaganapathy M, Raman N. Pharmacological activity of a few transition metal complexes: a short review. *J Chem Biol Therap.* 2016;1:108.
14. Hayder HM, Nesser KS. Synthesis, characterization of mixed ligand complexes containing 2,2-Bipyridine and 3-aminopropyltriethoxysilane. *J Phys.* 2018.
15. Festus C, Don-Lawson CD. Synthesis, spectral, magnetic and in-vitro biological studies of organic ligands and their corresponding heteroleptic divalent d-metal complexes. *The Pharmaceutical and Chemical Journal*. 2018;5:118–129.
16. Osowole AA, Festus C. Synthesis, spectral magnetic and antibacterial studies of some divalent metal complexes of 3-{[(4,6-dihydroxy pyrimidin-2-yl)Imino]methyl}Napthalen-2-ol. *Journal of Chemical Biological and physical sciences*. 2015;6:210–219.
17. Hong H, Kitaura J, Xiao W, et al. The Src family kinase Hck regulates mast cell activation by suppressing an inhibitory Src family kinase Lyn. *Blood*. 2007;110:2511–2519.
18. Festus C. Solvo-thermal Assisted-Synthesis; Experimental and Theoretical Characterization; and Biological Evaluations of Azo-Chelator-Ligand Chelates of Fe(II) and Zn(II) ions. *Asian Journal of Applied Chemistry Research.* 2021;10:40–56.
19. Festus C, Collins UI, Obinna O. Novel 3d divalent metallic complexes of 3-[(2-hydroxy-5-methylphenylimino)-methyl]-napthalen-2-ol: Synthesis, spectral, characterization, antimicrobial and computational studies. *Journal of Molecular Structure*. 2020;1210:1–13.
20. Nejo AA, Kolawole GA, Opoku AR. Synthesis, characterization and preliminary Insulin-enhancing studies of symmetrical tetradentate Schiff base complexes of oxovanadium(IV). *Inorganica Chimica Acta.* 2009;362:3993–4001.
21. Valarmathy G, Subbalakshmi R. Synthesis, spectral characterisation, electrochemical, and fluorescence studies of biologically active novel Schiff base complexes derived from E-4-(2-hydroxy-3-methoxybenzlideneamino)-N-(pyrimidin-2-yl)benzenesulfonamide. *Turkish Journal of Chemistry*. 2014;38:521–530.
22. Tarek MI, El-Ghamry MA, Abu-El-Wafa SM. et al. Synthesis, characterization, 3D-modelling, biological activities of some metal complexes of novel sulpha drug Schiff base ligand and its nano Cu complex. *Modern Chemistry: Science Publishing group.* 2015;3:18–30.
23. Dixit NS, Patel CC. Amine exchange reactions of mixed ligand nickel (II) complexes of Isonitroso-β-ketoimines. *Indian Journal of Chemistry*. 1979;17:1789–1991.
24. Festus C, Ekpete OA, Don-Lawson CD. Novel metal2+ complexes of N-(1,4-dihydro-1,4-oxonaphthalen-3-yl) pyrazine-2-carboxamide: Synthesis, structural characterization, magnetic properties and antimicrobial activities. *Curr Res Chem.* 2020;12:1–10.
25. Laxmi K, Pranya VJ, Tapan KD, et al. Reaction between lawsone and aminophenol derivatives: synthesis, characterization, molecular structures and antiproliferative activity. *J Mol Struct*. 2014;1075:397–405.
26. Chohan ZH. Synthesis, characterization and biological properties of bivalent transition metal complexes of Co(II), Cu(II), Ni(II), and Zn(II) with some acylhydrazine derived from furanyl and thienyl ONO and SNO donor Schiff base ligands. *Synth React Inorg Met org Chem.* 2001;31:1–6.
27. Atmaram KM, Kirian VM. Synthesis, characterization and antimicrobial activity of mixed Schiff base ligand complexes of transition metal(II) ions. *Intl J ChemTech Research.* 2011;3:477–482.

28. Osowole AA, Anthony CE, Benedict OA. Synthesis, spectroscopic characterisation and structure related antibacterial activities of some metal(II) complexes of substituted triflurobutenol. *Elixir International Journal.* 2013;59:15848–15852.

29. Cotton AF, Wilkinson G, Murillo CA. et al. *Advanced Inorganic Chemistry*. 6th Edn. Wiley publishers. 1999.

30. Nogrady T. *Medical Chemistry: A biochemistry approach*. Oxford University Press, New York. 1988.

31. Salmon L, Molnar G, Cobo S, et al. Reinvestigation of the spin crossover phenomenon in the ferrous complex $[Fe(HB(pz)_3)_2]$. *New Journal of Chemistry.* 2009;33(6):1283–1289.

32. Festus C, Wodi CT. Corrosion Inhibition; and Antimicrobial Studies of Bivalent Complexes of 1-(((5-ethoxybenzo[d]thiazol-2-yl)Imino) methyl)naphthalene-2-ol Chelator: Design, Synthesis, and Experimental Characterizations. *Direct Research Journal of Chemistry and Materials Science*. 2021;8:31–43.

33. Lofty K. Molecular Modeling, Docking and ADMET of Dimethylthiohydantoin Derivatives for Prostate Cancer Treatment. *Journal of Biophysical Chemistry*. 2015;6:91–117.

34. Khan SK, Rizwan K, Shahid S. et al. Synthesis, DFT, computational exploration of chemical reactivity, molecular docking studies of novel formazan metal complexes and their biological applications. *Applied Organometallic Chemistry*. 2019;34:1–24.

35. Philip S, Jayasree GE, Mohanan K. Antidiabetic, antioxidant, DFT and molecular docking studies of a triazene derivative and its transition metal complexes. *Research on Chemical Intermediates*. 2019;46:75–99.

36. Bououden W, Benguerba Y. Computational Quantum Chemical Study, Drug-Likeness and In Silico Cytotoxicity Evaluation of Some Steroidal Anti-Inflammatory Drugs. *Journal of Drug Delivery and Therapeutics*. 2020;10:68–74.

Citation: Chioma F, Nwoke IB, Valentine O. Synthesis; spectral, computational studies; and antimicrobial evaluations of Fe(II) and Zn(II) chelates containing R'C-NR" and N_2O_2 moieties. *J Anal Pharm Res.* 2022;11(2):45–54. DOI: 10.15406/japlr.2022.11.00401